Journal of Nuclear Research and Applications

Research Paper

Vol. 3, No. 2, P 32-48, Spring (2023)

Cited in: https://jonra.nstri.ir

Received: 14 February 2022, Accepted: 15 October 2022

RSM-based Investigation of Cesium Removal from Aqueous Media with Nanocomposites Prepared by Spherical Mesoporous Silica and Potassium Metal Hexacyanoferrate

Sh. Amin[1], S. A. Alavi[1], H. Yousefnia[2], H. Aghayan[3*]

[1]. *Department of Chemical Engineering, Science and Research Branch, Islamic Azad University, P.O. Box: 775-14515, Tehran, Iran*

[2]. *Radiation Application Research School, Nuclear Science and Technology Research Institute (NSTRI), P.O.Box: 14155-1339, Tehran – Iran*

[3]. *Materials and Nuclear Fuel Research School, Nuclear Science and Technology Research Institute (NSTRI), P.O.Box: 11365-8486, Tehran – Iran*

ABSTRACT

We investigated the effects of different variables on cesium adsorption from aqueous solutions using a synthesized nanocomposite. The surfaces of synthesized spherical mesoporous silica were modified with potassium hexacyanoferrate and characterized by different techniques including XRD, FT-IR, SEM, TGA, and BET/BJH. The response surface methodology based on the central composite design was used to optimize cesium ion adsorption conditions such as the effects of initial cesium concentration, contact time, temperature, and pH. The equilibrium concentration data were analyzed by Langmuir, Freundlich, and Tempkin isotherm models. The isotherm studies showed that monolayer adsorption isotherm (Langmuir) is consistent with the experimental data. Based on kinetic studies, Blanchard's pseudo-second-order reaction kinetics model provides the best correlation of the experimental data. The initial concentration and pH were the most influential factors in cesium adsorption. The result showed the nanocomposite adsorbed cesium ions selectively even in the presence of high Na^+, K^+, and Sr^{2+} ions.

***Keywords*:** Spherical SBA-15; Cesium; RSM; Hexacyanoferrate

1. Introductions

^{137}Cs ion, as a radioisotope of Cs, is a by-product of the fission process in nuclear reactors. Due to high fission efficiency, an average half-life of about 30 years, high-energy radiation, and high reactivity, ^{137}Cs is a hazardous product of fission [1-3]. Therefore, it is vital to remove ^{137}Cs from aqueous media. Numerous studies have examined the adsorption of these substances using a variety of methods [4-6]. By adsorbing heavy metals in water and industrial effluents, mesoporous compounds and functionalized mesoporous compounds are a suitable solution that has recently been proposed as a way to remove heavy metal contamination in water and industrial effluents [7-15]. Meanwhile, SBA-15 silica mesoporous with a silanol surface, first manufactured in 1998, has attracted the attention of many researchers because of having such improved properties as

*. *Corresponding Author name*: H. Aghayan
E-mail address: hasanaghayan @yahoo.com

efficient diameter and high strength. Stucky et al. first developed high-diameter silica mesoporous with a hexagonal cavity structure, known as SBA-15 [16]. Due to its suitable cavity width and other advantages (e.g., high thermal resistance and thicker wall diameter), this type of mesoporous composition is superior to other mesoporous compositions used in catalytic substrates, sensors, adsorbents, etc. [17,18].

A wide variety of SBA-15 morphologies such as the sphere, fiber, doughnut-like, rod, rice-shape, rope, egg-sausage, gyroid, platelet, and discoid-like shapes have been reported in the literature [19-22]. Among these morphologies, spherical structures perform more efficiently in separation processes and column operations due to their easier access to larger pores and slower molecular penetration. Despite this, they lack suitable surface properties for a wide variety of applications. To modify the surface properties and increase the adsorption capacity of spherical particles, hybrids with ion exchanger materials are a practical technique.

Metal hexacyanoferrates are known as specific cesium ion adsorbents. Potassium metal hexacyanoferrates (metal=transition metals such as Co, Cu, Ni, Zr, and Zn) have been extensively used due to satisfactory cesium removal from solutions. They can selectively adsorb cesium ions because of the similar structure lattice size and diameter of hydrated cesium ions. However, these complexes are composed of tiny crystals leading to low mechanical stability making them unsuitable for column applications. They also have a low surface area. [23-27].

As a solution to this problem, the complex is loaded onto a solid support (e.g. SBA-15), and the resulting composite is used as an exchange [28-30]. Design, as a significant part of engineering, is aimed at improving the performance of production processes. Different experimental design techniques are used to identify the influential factors of the process and determine the optimal values. The variables with the most substantial effect on the output can be identified by using the design of experiments (DOE). This technique can also extract the effective input variables so that the response values get closer to their nominal value, reduce their variability, and minimize the effect of uncontrollable factors on the response variable [31]. In this regard, the response surface method (RSM) is a reliable, efficient design method. The RSM was first proposed by Box and Wilson (1951) by modifying Taguchi's method [32]. The use of the RSM, as one of the most critical techniques for the design of experiments, has resulted in the development of several mathematical and statistical techniques, including statistical design of experiments, statistical modeling, and preliminary and proper optimization, utilized for new process development, production optimization, design improvement, and new product formulation [33]. The response surface method is used to solve some significant industrial and research problems [34,35]. In the RSM, experimental design is through some independent variables as inputs. Therefore, the relationship between one or more evaluated dependent variables can be determined by conducting an optimal number of experiments. In the present study, the adsorption of Cs from an aqueous medium was investigated using (SBA-15-) [$KCu(Fe(CN_6))$] adsorbent, and then the influential operating parameters of this process were optimized. The RSM with a central composite design (CCD) was used to evaluate the effect of temperature (C), time (h), Cs ion concentration (mg/L), and pH on five levels.

2. Experimental

2.1 Materials and Methods

Copper (II) nitrate trihydrate ($Cu(NO_3)_2{\cdot}3H_2O$), *Nickel* (II) *nitrate hexahydrate* ($Ni(NO_3)_2{\cdot}6H_2O$), *Cobalt* (II) *nitrate hexahydrate* ($Co(NO_3)_2{\cdot}6H_2O$), *Zirconyl chloride octahydrate* ($ZrOCl_2$), *Potassium*

hexacyanoferrate(II) *trihydrate* ($K_4[Fe(CN)_6].3H_2O$), *Cetyltrimethylammonium Bromide or CTAB* ($[(C16H33)N(CH_3)_3]Br$), *Tetraethyl orthosilicate or TEOS* $Si(OC_2H_5)_4$, pluronic p123 ($HO(CH_2CH_2O)_{20}(CH_2CH(CH_3)O)_{70}(CH_2CH_2O)_{20}H$), *Hydrochloric acid* (HCl), *Cesium nitrate* ($CsNO_3$), *Strontium nitrate* $Sr(NO_3)_2$, Sodium chloride (NaCl) and Potassium chloride (KCl) were purchased from Merck company.

2.2. Apparatus:

Cesium concentration was measured by atomic absorption spectrometer, PerkinElmer 843. The XRD patterns of samples were taken by Philips PW1130/90 instrument (wide angle) and Philips PW1730 instrument (low angle). The FT-IR spectra of samples were recorded between 400 and 4000 Cm^{-1} using a Brucher vector-22 spectrometer. The SEM images were prepared by Philips XL30 instrument. N_2- adsorption-desorption isotherms were prepared using Quantachrome NOVA 2200 e instrument. The thermal curves are taken by thermal analyzer model PL-STA 1500, PL Thermal science.

2.2.1. Synthesis of Spherical (SBA-15):

The synthesis of spherical SBA-15 was carried out through the following procedure: 0.5 g of CTAB was dissolved in 60 mL of HCl 2 M and 15 mL of distilled water. Then, 2 g of pluronic p123 was uniformly dissolved in the solution. After achieving a homogeneous solution, 5 mL of TEOS solution, as a silica source, was added slowly and dropwise and stirred at 40°C for 24 h. The solution was then transferred to an autoclave and dried in an oven at 100° C for 24 h. The obtained powder was calcinated to 550°C. This temperature was held for 6 h to remove surfactants and stabilize the structure. The increasing temperature gradient was 1°C/min [36].

2.2.2. Synthesis of (SBA-15)-[KX(Fe(CN)$_6$)] nanocomposite:

To prepare (SBA-15)-[$KX(Fe(CN)_6)$] nanocomposite (X=Cu, Ni, Co, and Zr), 1 g of (SBA-15) in 60 ml of the solution of metal salts $Cu(NO_3)_2.3H_2O$, $Ni(NO_3)_2.6H_2O$, $Co(NO_3)_2.6H_2O$ and $ZrOCl_2.8H_2O$ (1M) was stirred for three h. Next, the product was separated from the solution, rinsed with distilled water, and dried out at 100°C for three h. The functionalized (SBA-15) was then stirred for 3 h with 1M solutions of $[K_4Fe(CN)_6]$ to form $[KX(Fe(CN)_6]$ (X=Cu, Ni, Co, and Zr) on (SBA-15) support. In the next stage, the product was rinsed and dried out at 90°C for three h.

2.3. Investigation of Cs adsorption by (SBA-15) -[YX(Fe (CN)$_6$)] nanocomposites:

Ferrocyanide has a great tendency to adsorb alkali metals, particularly Cs. Various composites of transition and alkali metals were produced from such hexacyanoferrates as [YX ($Fe(CN_6)$)], in which Y is the alkali metal and X is the transition metals (Co, Cu, Ni, and Zr). Hexacyanoferrate compounds in the form of [$KX(Fe(CN_6))$], have been shown the highest cesium selectivity and adsorption efficiency [37]. Since this study aimed to increase the efficiency of these composites by modifying their structure and immobilizing them on a support, the role of the transition metals in increasing Cs adsorption in these composites was investigated. For this purpose, the experiments were carried out with 0.1 g of the different synthesized nanocomposite, 20 ml of 100 ppm Cs solution at pH=6, a temperature of 25 °C, and a duration of 24 h.

The efficiency of cesium adsorption by nanocomposite was calculated by Equation 1.

$$R=\frac{C_0-C_t}{C_0}\times 100 \quad (1)$$

where R is the percentage of cesium adsorption, C_0 is the initial concentration of cesium in mg/L, C_t is the cesium concentration in sampling times t and in mg/L. The calculated values for the absorption rate (response variable) have been shown in Table 111.

Also, the equilibrium capacity of adsorption was calculated by equation 2.

$$q_e=\frac{(C_0-C_e)V}{W} \quad (2)$$

In this relation, q_e is the equilibrium capacity of adsorption in mg/g, C_0 is the initial concentration of cesium in mg/L, C_e is the equilibrium concentration of cesium in mg/L, V the solution volume in mm, and W is the adsorbent mass in g.

According to the results, the highest efficiency of cesium adsorption by synthesized nanocomposites was 83% belonged to (SBA-15)-[KCu(Fe(CN)$_6$)], and the lowest 60% belonged to (SBA-15)-[KNi(Fe(CN)$_6$)]. Adsorption efficiency for (SBA-15)-[KCo(Fe(CN)$_6$)] and (SBA-15)-[KZr(Fe(CN)$_6$)] were 73% and 71% respectively. Therefore, based on these results, the experiments were continued using the (SBA-15)-[KCu(Fe(CN)$_6$)].

2.4. Layer by layer loading of [KCu(Fe(CN)$_6$)] on the (SBA-15) support:

Layer-by-layer loading of potassium copper hexacyanoferrate on (SBA-15) support was done through the following strategy:

1 g of (SBA-15) was stirred in 60 ml of 1 M copper nitrate solution for 3 hours to load copper on (SBA-15). The functionalized (SBA-15) was then separated from the copper nitrate solution, eluted, and dried at 90° C. The collected copper nitrate solution was stored to be used in the next stage. The obtained functionalized (SBA-15) was stirred with 1 M potassium hexacyanoferrate solution for three h, then separated from the potassium hexacyanoferrate solution, eluted, and dried at 90° C. The collected potassium hexacyanoferrate solution was stored to be used in the next stage. In this step, (SBA-15)-[KCu(Fe(CN)$_6$)] ^{I} nanocomposite was obtained. Other steps were performed as in step 1. In order to obtain the maximum amount of cesium absorption and the optimal amount of loading of [KCu(Fe(CN)$_6$)] compound on the (SBA-15) support, loading of [KCu(Fe(CN)$_6$)] was performed layer by layer and in 5 step as described. The optimal layer was layer 4 because the adsorption efficiency did not increase as the layer increased. Adsorption experiments were performed with 0.05 g of synthesized nanocomposite at pH = 7, initial concentration of cesium solution = 100 ppm, and duration of 24 hours at room temperature. The results are shown in Table 1.

Table 1. The effect of layer by layer loading of [KCu(Fe(CN)$_6$)] on spherical SBA-15 support on cesium ion adsorption efficiency.

Number of loading	Adsorption (%)
1	30
2	44
3	56
4	67
5	65

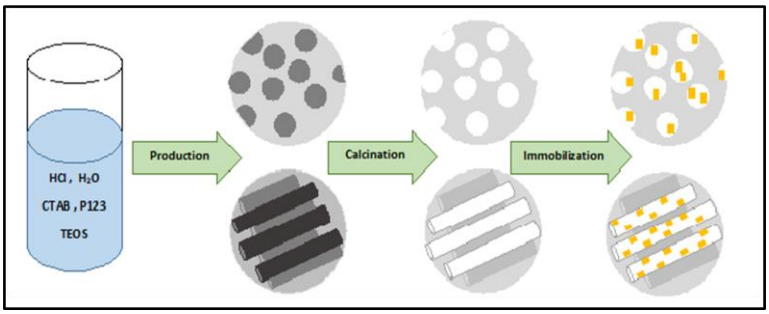

Scheme 1. Synthesis of Spherical mesoporous (SBA-15) and immobilization of [KMFe(CN)$_6$] on (SBA-15) support.

3. Results

3.1. Characterization

3.1.1. XRD patterns

The mesoporous SBA-15 and (SBA-15)-[KCu(Fe(CN)$_6$)] XRD patterns in low angles of the resulting samples are presented in Figure 1. These samples have a peak in the range of 0.5 and 2 corresponding to the plane (100) of the bi-dimensional p6mm hexagonal symmetry of the pores of SBA-15. However, after immobilization of KCu(Fe(CN)$_6$) on the support, the intensity of peaks becomes weaker and shift to a higher degree, which was indicative of the reduction in X-ray contrast as the empty pores were filled by hexacyanoferrate compounds [36,38,39]. In the wide-angle XRD pattern of (SBA-15)-[KCu(Fe(CN)$_6$)] at the scan range 2θ of 10°-80° (Figure 1), The well-defined lines corresponded to the diffraction planes of (200), (220), (400) were identical to the reference [KCu(Fe(CN)].

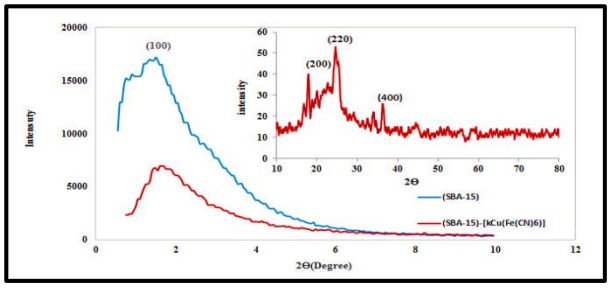

Fig 1. Low angle XRD patterns of SBA-15 and (SBA-15)- [KCu(Fe(CN)$_6$)]. The inset shows wide-angle XRD patterns of synthesized (SBA-15)-[KCu(Fe(CN)$_6$)] nanocomposite.

3.1.2. FT-IR spectra:

Figure 2 shows the FTIR spectrum of the mesoporous SBA-15 and (SBA-15)-[KCu(Fe(CN)$_6$)]. The characteristic absorption bands of Si–O–Si appeared at 464.01, 803.71 cm^{-1}. The band at 957.26 cm^{-1} was observed in the stretching vibration mode of Si-OH. The absorption band at 1632.15 cm^{-1} was observed at the bending vibration of O–H. The wide absorption band was observed in the stretching vibration mode of hydroxyl groups and silanol groups. In the mesoporous (SBA-15)-[KCu(Fe(CN)$_6$)] spectrum, the bands of Si–O–Si were observed at 460.94, and 789.66 cm^{-1}. The band at 957.52 cm^{-1} was observed in the stretching vibration mode of Si-OH. The absorption band at 1637.39 cm^{-1} was observed at the bending vibration of O–H. Moreover, the absorption bands at 470.09 cm^{-1} and 2080.98 cm^{-1} were observed in the Cu–C stretching mode and Fe–CN-Cu deformation mode, respectively.

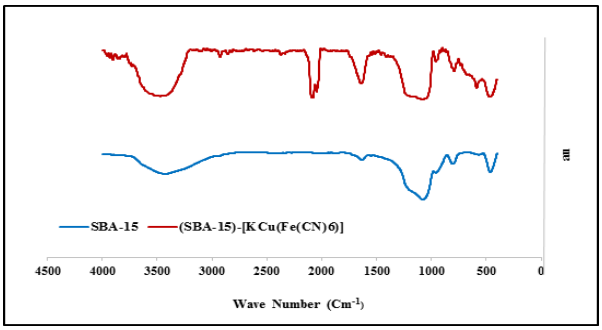

Fig 2. FT-IR spectra of (-) synthesized (SBA-15) and (-) synthesized (SBA-15)-[KCu(Fe(CN)$_6$)] nanocomposite.

3.1.3. SEM images

SEM imaging technology was also used to evaluate the surface of mesoporous SBA-15 .The SEM images indicate the spherical distribution of particles with mainly free standing spheres, but in some cases, aggregation was also observed. Moreover, the mean size of synthesized SBA-15 was approximately between 2-5µm (Figure 3).

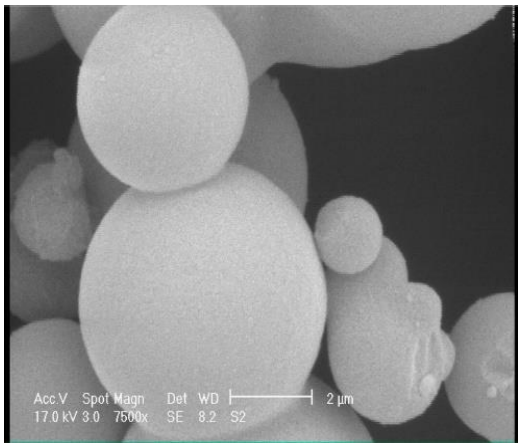

Fig 3. SEM image of the synthesized (SBA-15).

3.1.4. BET Surface Area

The BET method was used to calculate the specific surface areas of the SBA-15 and (SBA-15)-[$KCu(Fe(CN)_6)$]. The pore size distributions and pore volumes BJH equation were used to evaluate the pore structures. Figure 4 shows the samples' N_2 adsorption-desorption isotherms. According to the IUPAC classification, these isotherms are type IV isotherms for mesoporous materials [40]. As shown

in Figure 4, there is a capillary compression step at the SBA-15 adsorption and desorption isotherms with high curvature at relative pressures between 0.6 and 0.7, indicating similar mesopores. This feature is confirmed by the presence of a hysteresis loop, H1 type, in this diagram. In the curve corresponding to (SBA-15)-[$KCu(Fe(CN)_6)$], the hysteresis loop shifts to lower relative pressures and shows a decrease in the amount of nitrogen adsorbed, which expresses the loading of [$KCu(Fe(CN)_6)$] Inside the pores. Table 2 presents the BET results, according to which the surface area, pore volume, and mean pore diameter of the nanocomposite reduced with loading [$KCu(Fe(CN)_6)$] on SBA-15.

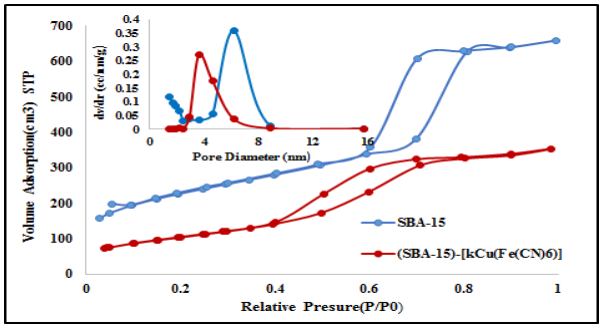

Fig 4. N_2 adsorption/desorption isotherm of (SBA-15) and (SBA-15)-[$KCu(Fe(CN)_6)$]. The inset shows the BJH pore-size distribution calculated from the desorption branch of the isotherms.

Table 2. Results of BET/BJH analysis for SBA-15 and (SBA-15)-[$KCu(Fe(CN)_6$].

Samples	a_S, BET ($m^2\ g^{-1}$)	Total pore volume ($cm^3\ g^{-1}$)	Mean pore diameter (nm)
SBA-15	806	0.98	6.2
(SBA-15)-[$KCu(Fe(CN)_6$)]	461	0.56	4.6

3.1.5. Thermal Curves

The temperature stability of this mesoporous was examined by thermal gravimetric analysis of the corresponding curves synthesized nanocomposite, the thermal curves (TGA) of mesoporous SBA-15 and (SBA-15)-[$KCu(Fe(CN)_6)$] were investigated. The TGA analysis SBA-15 shows the loss of mass (about 3%) between room temperature and 200ºC that is related to physically adsorbed water molecules, which is an endothermic process. On the other hand, in the (SBA-15)-[KCu(Fe(CN)6)] one can see different behavior in comparison with

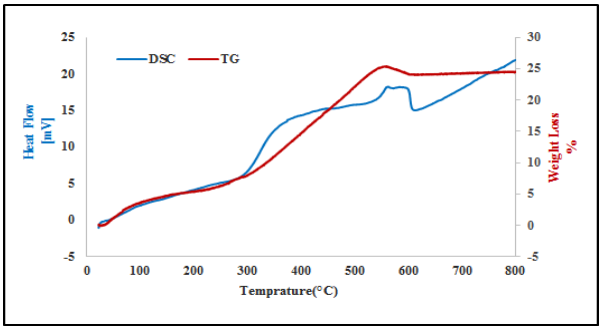

Fig 5. TG-DSC curves of synthesized SBA-15.

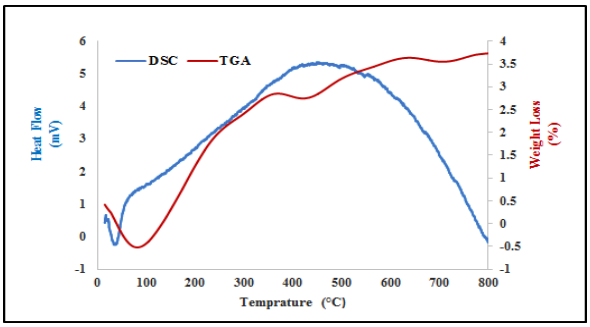

Fig 6. TG-DSC curves of synthesized (SBA-15)-[$KCu(Fe(CN)_6$] nanocomposite.

3.2. Design of Experiments

Design of Experiments is a convenient method for obtaining accurate information from the studied variables. The most significant advantages of the Design of Experiments are the ability to demonstrate the interaction of variables while saving time and money on experimentation. Design of Experiments based on the Response Surface Methodology is a set

of statistical techniques and applied mathematics for modeling the experimental data introduced by Box and Wilson [32] and has only been used as a powerful tool for the Design of Experiments. The Response Surface Methodology consists of four major stages: selecting the Design of the Experiment (Box-Behnken, Central Composite, Factorial, Taguchi, D-optimal) and conducting experiments, statistical analysis of experimental data obtained through the appropriate polynomial function, evaluating the model (via indicators and graphs), and obtaining the optimal values for the studied variables [33].

One of the most common Response Surface Methods is the central composite design [33,41]. The central composite design is divided into five surfaces: +α, -α, 0, +1, and, -1. Designing using the central composite method typically has K variables and is divided into three parts.

1. Complete two-level factorial design in which the number of experiments is generally obtained by $N_f = 2^K$. The points of the Two-level factorial design are on +1 and -1 surfaces.
2. The star design is used to estimate the curvature of the star points, and the number of experiments is Ns = 2K in this case. The points of the star design are on +α and -α levels.
3. Central points are points that are repeated and are precisely located in the center of the design. These repetitions are used to estimate the experimental error and measure the fit's weakness. The points are on zero surfaces.

The total number of experiments will be calculated by adding parts 1 through 3.

ANOVA is used to evaluate the model and analyze data, determining the P-value, F-value, Lack of fit, and Correlation Coefficient (R^2). The F-value measures the data deviation from the mean value and is used to determine the model's significance. The larger the numerical value, the more significant the model is.

P-value is an indicator used to determine the significance of variables; in general, values less than 0.05 indicate that the variables are significant, while values greater than 0.1 indicate that the variables are not significant. Lack of fit is an indicator that confirms the model's high accuracy in predicting estimated values and the low importance of the omitted variables for each experiment. In other words, the insignificant lack of fit implies that the difference between the actual values and the prediction is insignificant. R^2 demonstrates the correlation between the experimental and predicted values by the model, confirming model validation.

In this study, the Design Expert version 11 was used to design the experiments. The design of experiments was based on the central composite design. Based on this method, 30 experiments were conducted with four independent variables of initial solution concentration, contact time, temperature, and pH at five levels, and removal efficiency as the dependent variable (response), as shown in Tables 3 and 4.

Table 3. Independent variables and their levels in the experimental.

Independent variables	Coded symbols	Levels
Temperature (°C)	A	25 35 45 55 65
Time(h)	B	0.5 6.38 12.25 18.13 24
Concentration(mg/L)	C	10 257.5 505 752.5 1000
pH	D	3 5 7 9 11

The experiments were carried out in accordance with the design of experiments shown in Table 4, using 0.05 g of nanocomposite to investigate the effect of variables on the process of cesium adsorption by nanocomposite. The samples were then filtered, and the concentration of cesium ion was measured before and after each experiment using atomic absorption spectroscopy, and the cesium adsorption efficiency was calculated using Equation 1. Table 4 displays the calculated values for the absorption efficiency (response variable).

Table 4. The central composite design experiment for the 4 independent variables and results for Cs^+ adsorption efficiency.

STD	Run	Temperature (ºC)	Time (h)	Concentration (ppm)	pH	Efficiency (%)
16	1	55.00	18.13	752.50	9.00	16
14	2	55.00	6.38	752.50	9.00	10
15	3	35.00	18.13	752.50	9.00	14
23	4	45.00	12.25	505.00	3.00	10
21	5	45.00	12.25	10.00	7.00	89
27	6	45.00	12.25	505.00	7.00	24
1	7	35.00	6.38	257.50	5.00	40
17	8	25.00	12.25	505.00	7.00	23
7	9	35.00	18.13	752.50	5.00	12
13	10	35.00	6.38	752.50	9.00	12
18	11	65.00	12.25	505.00	7.00	28
26	12	45.00	12.25	505.00	7.00	24
2	13	55.00	6.38	257.50	5.00	44
12	14	55.00	18.13	257.50	9.00	50
10	15	55.00	6.38	257.50	9.00	46
8	16	55.00	18.13	752.50	5.00	11
24	17	45.00	12.25	505.00	11.00	21
22	18	45.00	12.25	1000.00	7.00	8
30	19	45.00	12.25	505.00	7.00	21
25	20	45.00	12.25	505.00	7.00	23
20	21	45.00	24.00	505.00	7.00	25
6	22	55.00	6.38	752.50	5.00	6
29	23	45.00	12.25	505.00	7.00	24
9	24	35.00	6.38	257.50	9.00	44
3	25	35.00	18.13	257.50	5.00	44
19	26	45.00	0.50	505.00	7.00	25
11	27	35.00	18.13	257.50	9.00	46
28	28	45.00	12.25	505.00	7.00	20
4	29	55.00	18.13	257.50	5.00	48
5	30	35.00	6.38	752.50	5.00	10

The proposed model for the cesium adsorption efficiency based on the coded variables was presented as a quadratic polynomial using the response surface methodology as follows:

$$Y = 22.67 + 0.7917 \times A + 1.21 \times B - 18.04 \times C + 1.88 \times D + 0.5625 \times A \times B - 1.19 \times A \times C + 0.1875 \times A \times D + 0.0625 + 0.0625 \times B \times C - 0.0625 \times B \times D + 0.1875 \times C \times D + 0.6563 \times A^2 + 0.5313 \times B^2 + 6.41 \times C^2 - 1.84 \times D^2.$$

In this relation; Y indicates the efficiency of cesium removal (response variable) and is a function of A, B, C, and D corresponding to the temperature, time, initial concentration of the solution, and pH, respectively; the cesium removal efficiency was evaluated by adding a fixed number, first degree effects (A, B, C, and D), interactions (AB, AC, AD, BC, BD, and CD) and quadratic effects (A_2, B_2, C_2, and D_2).

Table 5 contains the results of an analysis of variance (ANOVA) performed to ensure the model's efficiency.

According to Table 5, the F-value and P-value for this model were 91.21 and <0.0001, respectively, confirming that this model is statistically significant. The P-value for time variables (B), concentration (C), pH (D), concentration-temperature interaction (AC), quadratic concentration variable (C^2), and quadratic pH (D^2)

was less than 0.05, indicating the significance of the variables. The F-value for these parameters indicates that the most influential variable in the process of cesium adsorption is the initial concentration of the solution. The correlation coefficient (R^2 = 0.9884) indicates a good match between the experimental and predicted data by the model. The closer this value is to one, the more accurate the model is. The P-value (0.1139) for Lack of Fit was not significant, indicating the lower importance of the deleted variables and the high accuracy of the model. Figure 7 depicts the relationship between the predicted removal efficiency and the actual values based on the statistical model. As shown in this chart, the model can accurately predict experimental data in the range of independent variable changes.

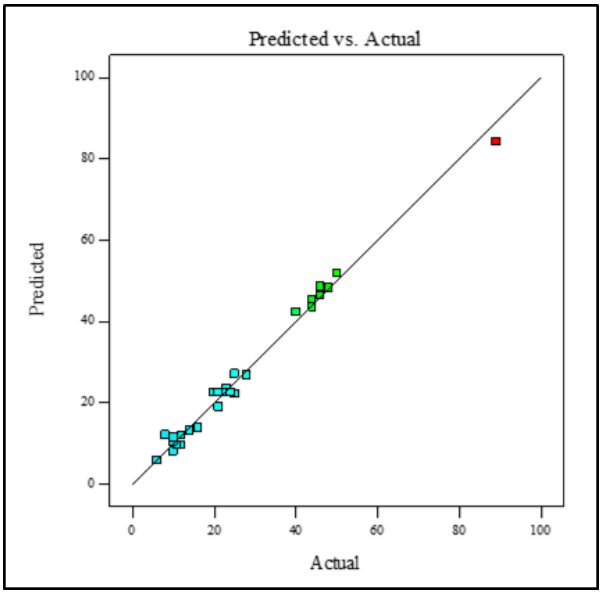

Fig 7. Experimental data versus calculated data by CCD method for Cs^+ adsorption by the synthesized (SBA-15)-[$KCu(Fe(CN)_6)$] nanocomposite.

Table 5. Analysis of variance (ANOVA) and adequacy of the quadratic model for Cs^+ adsorption by the synthesized.

Source	Sum of squares	Degree of freedom	Mean square	F-value	P-value Prob >F
Model	9314.45	14	665.32	91.21	< 0.0001 significant
A-Temperature	15.04	1	15.04	2.06	0.1715
B-Time	35.04	1	35.04	4.80	0.0446
C-Concentration	7812.04	1	7812.04	1070.96	< 0.0001
D-pH	84.38	1	84.38	11.57	0.0039
AB	5.06	1	5.06	0.6940	0.4179
AC	22.56	1	22.56	3.09	0.0990
AD	0.5625	1	0.5625	0.0771	0.7850
BC	0.0625	1	0.0625	0.0086	0.9275
BD	0.0625	1	0.0625	0.0086	0.9275
CD	0.5625	1	0.5625	0.0771	0.7850
A^2	11.81	1	11.81	1.62	0.2226
B^2	7.74	1	7.74	1.06	0.3193
C^2	1125.67	1	1125.67	154.32	< 0.0001
D^2	93.24	1	93.24	12.78	0.0028
Residual	109.42	15	7.29		
Lack of Fit	94.08	10	9.41	3.07	0.0081 not significant
Pure Error	15.33	5	3.07		
Correction total	9423.87	29			

(SBA-15)-[$KCu(Fe(CN)_6)$] nanocomposite

3.2.1. Effect of Initial concentration of Cs, Contact time, Temperature, and pH on Adsorption Efficiency

Figures 8-10 are the three-dimensional representation of the effect of temperature, time, cesium ion concentration, and pH on Cs ion adsorption efficiency.

3.2.1.1. Initial concentration

Initial concentration is one of the parameters that influence adsorption efficiency. As shown in Figure 8, increases in initial concentration reduced the adsorption efficiency of cesium ions by the synthesized (SBA-15)-[$KCu(Fe(CN)_6)$] nanocomposite. The reason for this decrease was the constant number of active adsorption sites for a constant adsorbent dosage. In other words, we can say that less adsorbate was adsorbed at higher concentrations due to the lower ratio of active sites to the concentration of Cs ions. In contrast, adsorption capacity improved at higher concentrations due to the increased probability of collision between Cs ions and the surface area of the adsorbent. In addition, increases in concentration were accompanied by a higher driving force for mass transfer, and hence Cs infiltration into the layers of the solution surrounding the adsorbent was greater. Consequently, for a given adsorbent dosage, increases in concentration improved adsorption capacity to the point when all the available active sites of the adsorbent were occupied. The highest adsorption capacity for the mentioned adsorbent was 46.4 mgg^{-1}.

3.2.1.2. Contact time

Figures 8 and 9 indicate that contact time did not have a significant impact on adsorption efficiency as about 90% of the Cs ions were adsorbed in the first 30 minutes of the adsorption process by the synthesized (SBA-15)-[$KCu(Fe(CN)_6)$] nanocomposite and increases in contact time did not tangibly influence adsorption. This high and fast adsorption of Cs ions was due to the presence of a large number of vacant active sites available to the nanocomposite and also because of the large concentration gradient for the Cs ions at the beginning of the process. The adsorption rate decreased and eventually became constant with the time, occupation of the active sites, and reduction in concentration gradient.

3.2.1.3. Temperature

According to Figures 9 and 10, the amount of Cs ions adsorbed by the synthesized (SBA-15)-[$KCu(Fe(CN)_6)$] nanocomposite increased at higher temperatures indicating that the adsorption process was endothermic. The activity of the nanocomposite surface and the kinetic energy of the solution increased as the temperature was raised. In addition, improved adsorption at higher temperatures could be due to reduction in the thickness of the boundary layer around the nanocomposite that decreased resistance to the transfer of the mass of cesium ions in the boundary layer.

3.2.1.4. pH

pH is an important factor in adsorption processes because it influences the interactions between the adsorbent and the adsorbate. As shown in Figure 10, the adsorption of Cs ions increased when pH was raised to about 10. This increase could probably be due to the increase in the negative charge on the nanocomposite surface, which caused electrostatic interactions on its surface, resulting in higher adsorption of the positively charged Cs ions. At very acidic pH values, the hydrogen ions present in the solution competed with the metal ions for the occupation of the adsorption sites, thus reducing the adsorption of the metal ions. The decline in Cs adsorption at pH values higher than 10 could also result from metal ion complexation with the hydroxyl anions present in the solution at this pH range. This complexation

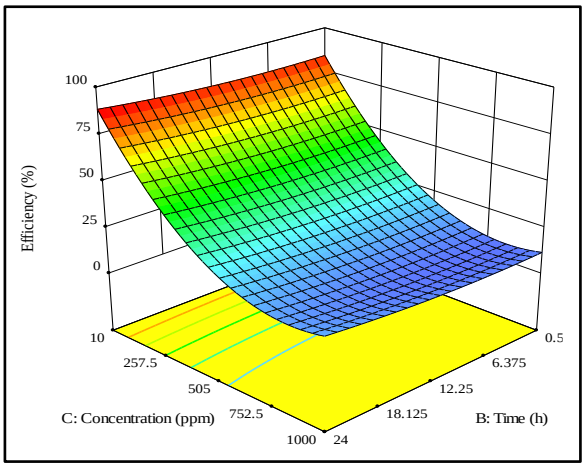

Fig 8. 3D plot of Cs^+ adsorption by (SBA-15)-[$KCu(Fe(CN)_6$)].The effect of Concentration Time on Cs^+ adsorption efficiency.

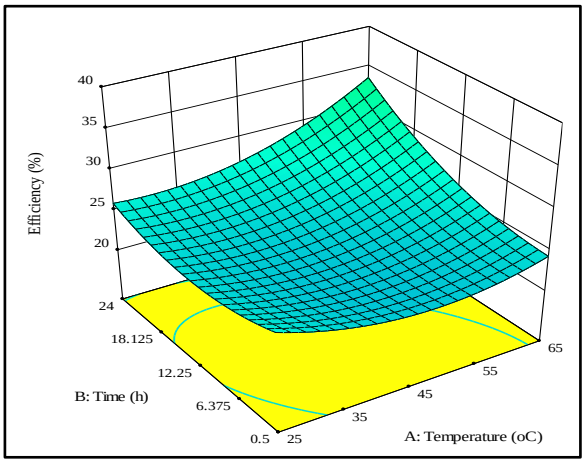

Fig 9. 3D plot of Cs^+ adsorption by (SBA-15)-[$KCu(Fe(CN)_6$)].The effect of Temperature-Time on Cs^+ adsorption efficiency.

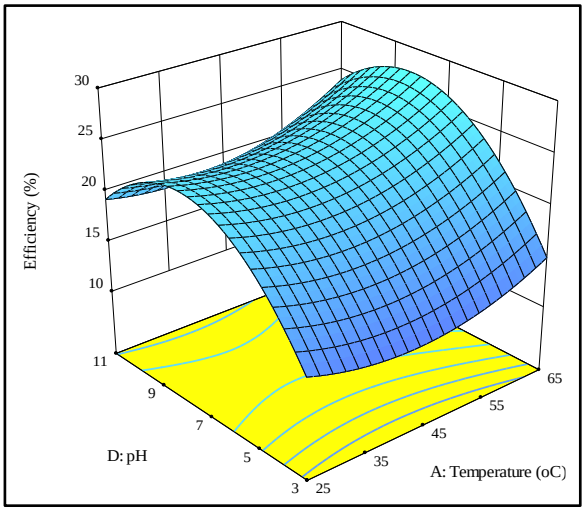

Fig 10. 3D plot of Cs^+ adsorption by (SBA-15)-[$KCu(Fe(CN)_6$)].The effect of pH- Temperature on Cs^+ adsorption efficiency.

caused the formation of new species of metal cations with chemical activity somewhat less than that of free cations, thereby reducing adsorption associated with the chemical activity of the species.

3.2.2. Determination of Optimal Conditions

Optimal conditions were specified by Design Expert software as follows: T = 65 ° C, t = 0.5 h, C = 18 ppm, and pH = 10. All variables were set in the range, and the response variable was set in the maximize. The maximum predicted cesium removal rate was 89%, which was well-matched to the experimental value.

3.3. Kinetic study

The study of adsorption kinetics provides information about the reaction path, mechanism, and adsorption rate [42,43]; for these means, Lagergren, Elovich, and Blanchard's kinetic models were employed [42-45].

3.3.1. Lagergren Equation

Lagergren proposed the following pseudo-first-order rate equation:

$$\ln(q_e - q_t) = \ln q_e - k_1 t \qquad (3)$$

q_e and q_t (mgg^{-1}) are the amounts of adsorbed material at equilibrium and time t, respectively; k_1 (min^{-1}) is the constant rate of pseudo-first-order adsorption.

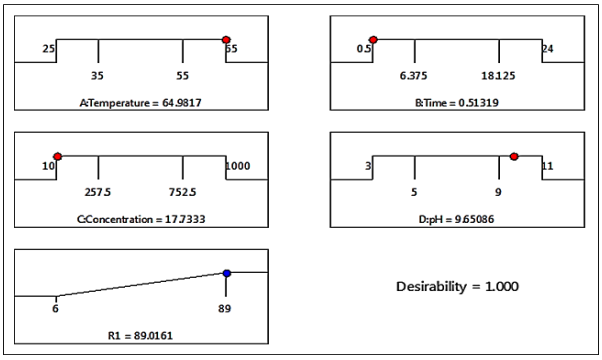

Fig 11. Optimum conditions of Cs^+ adsorption by the synthesized (SBA-15)-[$KCu(Fe(CN)_6$)] nanocomposite.

3.3.2. Elovich equation

The Elovich equation is another adsorbent capacity-based rate equation. In this equation, by using the boundary conditions (q_t = 0 at t = 0 and q_t= q_t at t = t), the following equation is obtained:

$$q_t = \frac{1}{\beta}\ln(\alpha\beta) + \frac{1}{\beta}\ln(t) \quad (4)$$

Where α is the initial adsorption rate constant (mol.g^{-1} min^{-1}), and β is the desorption rate constant (g. mol^{-1}) during the experiment.

The Elovich equation is mainly used to measure the kinetics of liquid adsorption on heterogeneous solids.

3.3.3. Blanchard equation

Blanchard proposed a pseudo-second-order rate equation to calculate ion exchange reactions. McKay and Ho defined the following linear pseudo-second-order rate equation:

$$\frac{t}{q_t} = \frac{1}{k_2 q_e^2} + \frac{1}{q_e}t \quad (5)$$

k_2 (g.mg^{-1}.min^{-1}) is the rate constant of pseudo-second-order equation.

The kinetic values of the respective parameter are given in Table 6. The kinetic studies showed that Blanchard's kinetic model provides the best correlation of the experimental data (R^2=0.9975).

3.4. Isotherms study

Adsorption isotherms are equilibrium data that show the reaction mechanisms of adsorbents. Isotherms can also be used to show the adsorption capacity of an adsorbent. The adsorption isotherms display the distribution equilibrium of the adsorbates between the solution phase and solid adsorbent phase. In addition, they can provide some physicochemical parameters that can express the adsorbent's affinity to the adsorbate [46].

This study used Langmuir, Freundlich, and Tamkin's isotherm models to analyze the experimental data and describe the equilibrium adsorption state between solid and liquid phases [42,43,46]. The model adherence was evaluated by plotting the curve for each isotherm and examining the model's coefficient of correlation R^2 with the experimental results.

3.4.1. Langmuir isotherm

The Langmuir isotherm is a model based on scientific hypotheses. The binding of the adsorbed material to specific and uniform points on the adsorbent surface, causing the occurrence of a single-layer adsorption process, is among the most important hypotheses in this regard.

This model also posits that all the adsorption sites are similarly coherent with the adsorbent molecules; in addition, the transfer of the adsorbent material does not occur at the adsorbent surface.

Table 6. Constants and correlation coefficient of kinetic models.

Model	Equation	Parameters(units)	R^2
Logergern	$\ln(q_e - q_t) = \ln q_e - k_1 t$	q_e= 17.70 (mgg^{-1}) k_1= 0.012 (min^{-1})	0.9535
Elovich	$q_t = \frac{1}{\beta}\ln(\alpha\beta) + \frac{1}{\beta}\ln(t)$	α = 69.29 (mol.g^{-1} min^{-1}) β = 0.203 (gmol^{-1})	0.9788
Blanchard	$\frac{t}{q_t} = \frac{1}{k_2 q_e^2} + \frac{1}{q_e}t$	q_e = 42.6 (mgg^{-1}) k_2= 0.0014 (gmg^{-1}min^{-1})	0.9975

The following equation presents this model:

$$q_e = \frac{q_m \times b \times C_e}{1 + b \times C_e} \quad (6)$$

b is Langmuir constant; q_e is the amount of the absorbed Cs, which in this equation is the equilibrium concentration of the solution (mg/L) for a given amount of adsorbent consumed (mg/g); and q_m represents the maximum amount of cesium adsorption (mg/g).

3.4.2. Freundlich isotherm

Freundlich isotherm is an empirical model that assumes nonuniform adsorption on the adsorbent surface and is shown by the following equation:

$$q_e = K_f C_e^{1/n} \quad (7)$$

In this equation, K_f and 1/n represent, respectively, the Freundlich adsorption constants of adsorption capacity and intensity.

34.3. Temkin Isotherm

The Temkin model modified the surface adsorption theory by considering the possible adsorbent-adsorbate interactions. As a result, the adsorption heat of all molecules in the adsorption layer decreases linearly due to increasing surface coating.

$$q_e = B_T \times ln(A_T \times C_e) \quad (8)$$

That B_T represents absorption energy and is equal to the absolute temperature (K); A_T represents a constant equilibrium bond (L/mg).

These isotherm models are expressed in terms of two main parameters, including the equilibrium capacity of adsorption (q_e) and the equilibrium adsorbate concentration (Ce), as shown in Figure 12.

Equilibrium adsorption data were consistent with Langmuir, Freundlich, and Tamkin adsorption isotherms. Table 7 shows the fixed coefficients and correlation coefficients of the studied isotherms. Correlation coefficients of each of the isotherms showed that Langmuir's model was the most appropriate model to describe the adsorption phenomenon under study and indicate a homogeneous distribution of active sites on the surface.

Table 7. Isotherm models and parameters for the Cs+ adsorption by the synthesized (SBA-15)-[$KCu(Fe(CN)_6)$] nanocomposite.

Model	Equation	Parameters(units)	R^2
Langmuir	$q_e = \frac{q_m \times b \times C_e}{1 + b \times C_e}$	q_m=42.10 (mg/g) b= 0.81 (L/mg)	0.9919
Freundlich	$q_e = K_f C_e^{1/n}$	K_f=9.8 (L/g) n=4.16	0.9393
Temkin	$q_e = B_T \times ln(A_T \times C_e)$	B_T=1.6 (L/mg) A_T=3.8 (mg/ L)	0.9262

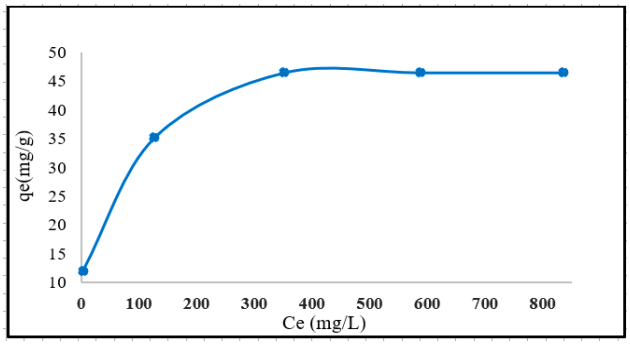

Fig 12. The plot of q_e v+ersus C_e for adsorption of Cs^+ by synthesized (SBA-15)-[$KCu(Fe(CN)_6)$] nanocomposite.

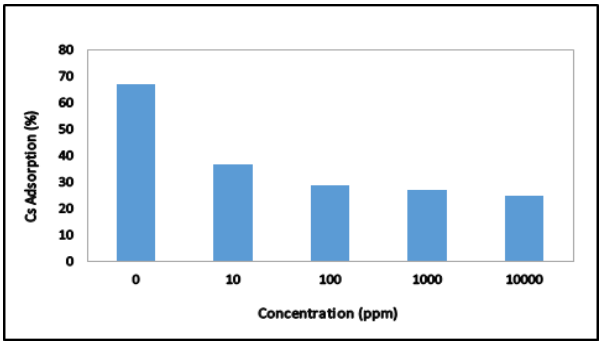

Fig 13. Cs^+ adsorption by the synthesized (SBA-15)-[$KCu(Fe(CN)_6)$] nanocomposite in the presence of Na^+, K^+, and Sr^{2+}

3.5. Selectivity of the adsorbent:

Four solutions containing Cs^+, K^+, Na^+, and Sr^{2+} ions at various concentrations were prepared to investigate the impact of the selectivity of the synthesized composite for Cs ions. Potassium, sodium, and strontium ions are usually found together with Cs ions in nuclear effluents and are very similar to Cs ions in ionic charge, ionic radius, or both [41]. Adsorption experiments were performed using 0.05 g of the synthesized nanocomposite under T = 25°C, pH = 10, and t = 24 h. The initial concentration of Cs was 100 ppm, and those of the interfering ions in each solution were 10, 100, 1000, and 10,000 ppm, respectively. The results revealed that Na^+ and K^+ ions, whether at low or at high concentrations, were not adsorbed by the nanocomposite, whereas, as shown in Table 7, the amount of potassium increased in all the solutions. The increased amounts were utterly proportionate to the amount of Cs adsorption. Cs adsorption was replaced by the mechanism of exchanging ions with the potassium present in the crystal structure of potassium copper hexacyanoferrate resulting in the formation of a more stable structure [37]. At low concentrations, as shown in Table 8, strontium ions were adsorbed by the nanocomposite, probably due to the presence of hydroxyl and silanol groups on the surface of the nanocomposite.

Although the interfering ions were not adsorbed by the nanocomposite or were only adsorbed in small amounts, they had a negative effect on Cs adsorption. The reduction in Cs adsorption varying from 30% at low concentrations to 42% at high concentrations may have been due to the influence of the interfering ions on the surface potential and the partial decrease in surface charge. The reduction in electrostatic force decreased the interactions between the metal ions and the active sites. The higher the amounts of these interfering ions were, the fewer Cs were adsorbed. Despite the reduction in Cs adsorption in the presence of the interfering ions, the synthesized nanocomposite exhibited good selectivity for Cs even at high concentrations.

Table 8. Effect of interfering ions on Cs^+ adsorption by synthesized (SBA-15)-[$KCu(Fe(CN)_6)$] nanocomposite.

	Cs adsorption (%)	Sr adsorption (%)	Na adsorption (%)	increasing in the amount of K (%)
Solution 1	39	80	0	360
Solution 2	29	20	0	28
Solution 3	27	0	0	2.5
Solution 4	25	0	0	0.2

3.6. Regeneration of the Nanocomposite:

Experiments were carried out in five consecutive cycles using 0.1 M nitric acids solution for 24 h to study the recovery and reuse capability of the synthesized nanocomposite. Figure 14 shows the results. After five cycles of nanocomposite recovery, its removal efficiency declined from 67% to 11%. This decrease could be due to the clogging of the active sides or their dissolution in the acidic environment. Removal of radionucleotides loaded on adsorbents and reuse of these adsorbents are not important issues. Still, the recovery of these adsorbents attracts interest concerning their use for the inactive states of these metals [37].

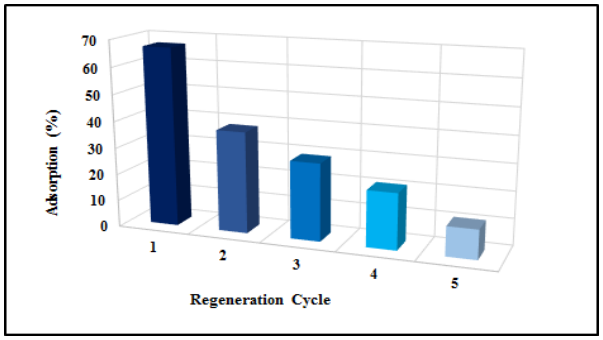

Fig 14. Nanocomposite regeneration cycle versus cesium adsorption efficiency.

4. Conclusions

This study investigated the adsorption of Cs^+ from an aqueous solution by synthesized (SBA-15)-[$KX(Fe(CN)_6)$] (X=Co, Cu, Ni, and Zr) nanocomposite. The RSM was used with a central composite design to optimize the operational variables (Temperature, Time, Concentration, pH) for the adsorption of Cs^+ by (SBA-15)-[$KCu(Fe(CN)_6)$]. The main factors affecting the adsorption efficiency were concentration and pH. The isotherm studies showed that monolayer adsorption isotherm (Langmuir) is consistent with the experimental data. Based on the results from kinetic studies, Blanchard's model of pseudo-second-order reaction kinetics provides the best correlation of the experimental data, and the synthesized nanocomposite adsorbed cesium ions selectively in the presence of Na^+, K^+, and Sr^{2+} ions.

Acknowledgments

The financial support of this study by the Nuclear Science and Technology Research Institute (NSTRI) and Science and Research Branch, Islamic Azad University is gratefully acknowledged.

References

1. Y. J. Gwon, et al., "*Prussian blue decoration on polyacrylonitrile nanofibers using polydopamine for effective Cs ion removal*". Industrial & Engineering Chemistry Research, **59**, 4872 (2020).
2. A. M. S. El-Din, T. Monir, M. A. Sayed, "*Nano-sized Prussian blue immobilized costless agro-industrial waste for the removal of cesium-137 ions*". Environmental Science and Pollution Research, **26**(25), 25550 (2019).
3. H. M. Yang, et al., "Hollow flower-like titanium ferrocyanide structure for the highly efficient removal of radioactive cesium from water". Chemical Engineering Journal, **392**, 123713 (2020).
4. J. Wang, S. Zhuang, "*Removal of cesium ions from aqueous solutions using various separation technologies*". Reviews in Environmental Science and Bio/Technology, **18**(2), 231 (2019).
5. S. Khandaker, et al., "*Development of synthetic zeolites from bio-slag for cesium adsorption: Kinetic, isotherm and thermodynamic studies*". Journal of Water Process Engineering, **33**, 101055 (2020).
6. Y. Hu, et al., "*Algal sorbent derived from Sargassum horneri for adsorption of cesium and strontium ions: equilibrium, kinetics, and mass transfer*". Applied microbiology and biotechnology, **103**(6), 2833 (2019).
7. J. A. S. Costa, et al., "*Synthesis, functionalization, and environmental application of silica-based mesoporous materials of the M41S and SBA-n families: A review*". Journal of Environmental Chemical Engineering, **9**, 105259 (2021).
8. Y. Shaochun, et al., "*Recent advances of SBA-15-based composites as the heterogeneous catalysts in water decontamination: A mini-review*". Journal of Environmental Management, **254**, 109787 (2020).

9. E. Vunain, A. K. Mishra, B. B. Mamba, "*Dendrimers, mesoporous silicas and chitosan-based nanosorbents for the removal of heavymetal ions*": A Review. International Journal of Biological Macromolecules, **86**, 570 (2016).

10. S. M. L. Santos, et al., "*Synthesis ans characterization of ordered mesoporous silica (SBA-15 and SBA-16) for adsorption of biomolecules*". Microporous and Mesoporous Materials, **180**, 284 (2013).

11. R. Narayan, et al., "*Mesoporous silica nanoparticles: a comprehensive review on synthesis and recent advances*". Pharmaceutics, **10**,118 (2018).

12. H. Wu, et al., "*Functionalization of SBA-15 mesoporous materials with 2-acetylthiophene for adsorption of Cr (III) ions*". Microporous and Mesoporous Materials, **292**, 109754 (2020).

13. M. A. Betiha, et al., "*Polyvinylpyrrolidone-Aminopropyl-SBA-15 schiff Base hybrid for efficient removal of divalent heavy metal cations from wastewater*". Journal of Hazardous Materials, **397**, 122675 (2020).

14. Y. Zhang, et al., "*Synthesis of pyridyl Schiff base functionalized SBA-15 mesoporous silica for the removal of Cu (II) and Pb (II) from aqueous solution*". Journal of Sol-Gel Science and Technology, **94**, 658 (2019).

15. E. Karakhanov, et al., "*Alkali earth catalysts based on mesoporous MCM-41 and Al-SBA-15 for sulfone removal from middle distillates*". ACS omega, **4**(7), 12736 (2019).

16. D. Zhao, et al., "*Triblock copolymer syntheses of mesoporous silica with periodic 50 to 300 angstrom pores*", Science, **279**, 548 (1998).

17. M. Kruk, et al., "*Characterization of the porous structureofSBA-15*". Chemistry of materials, **12**(7), 1961 (2000).

18. D. Zhao, et al., "*Morphological control of highly ordered mesoporous silica SBA-15*". Chemistry of materials, **12**(2), 275 (2000).

19. X. Liu, at al., "*Synthesis of large pore-diameter SBA-15 mesostructured spherical silica and its application in ultra-high-performance liquid chromatography*". Journal of Chromatography A, **1216**, 7767 (2009).

20. T. Yasmin, K. Muller, "*Synthesis and characterization of surface modified SBA-15 silica materials and their application in chromatography*". Journal of Chromatography A, **1218**, 6464 (2011).

21. M. Wang, et al., "*Study on adsorption mechanism of silicate adsorbents with different morphologies and pore structures towards formaldehyde in water*". Colloids and Surfaces A, **599**, 124887 (2020).

22. P. H. K. Charan, G. R. Rao, "*Textural and morphological studies of transition metal doped SBA-15 by co-condensation method*". Journal of Chemical Sciences, **127**, 909 (2015).

23. X. Liu, et al,. "*Adsorption removal of cesium from drinking waters: A mini review on use of biosorbents and other adsorbents*". Bioresource Technology, **160**,142 (2014).

24. R. saberi, et al., "*Adsorption characteristic of 137Cs from aqueous solution using PAN- based sodium titanosilicate composite*". Radioanalytical and Nuclear Chemistry, **284**, 461 (2010).

25. R. R. Sheha, "*Synthesis and characterization of mangnetic hexacyanoferrate (II) polymetric nanocomposite for separation of cesium from radioactive waste solution*". Colloid and Interface Science, **388** (1), 21 (2012).

26. A. Nilchi, et al., "*Adsorption of cesium on copper hexacyanoferrate- PAN composite ion exchanger from aqueous solution*", Chemical Engineering Journal, **172**, 572 (2011).

27. S. Vashnia, et al., "*Zinc hexacyanoferrate loaded mesoporous MCM-41 as a new adsorbent for cesium: equilibrium,kinetic and thermodynamic studies*". Desalination and Water Treatment, **55**, 1220 (2015).

28. S. Xiang, et al., "*Adsorption of cesium on mesoporous SBA-15 material containing embedded copper hexacyanoferrate*". Journal of Radioanalytical and Nuclear Chemistry, **320**(3), 609 (2019).

29. Y. K. Kim, et al., "*Solvent-assisted synthesis of potassium copper hexacyanoferrate embedded 3D-interconnected porous hydrogel for highly selective and rapid cesium ion removal*". Journal of environmental chemical engineering, **5**(1), 975 (2017).

30. M. Dashtinejad, et al., "*Synthesis, characterization, and cesium sorption performance of potassium nickel hexacyanoferrate-loaded granular activated carbon*". Particulate Science and Technology, **32**(4), 348 (2014).

31. W. J. Hill, W.G, Hunter, "*A Review of Response Surface Methodology: A Literature Survey*". Technometrics, **8**, 571 (1966).

32. S. Kotz, N. L. Johnson (Eds.), "*Breakthroughs in Statistics, Springer Series in Statistics (Perspectives in Statistics)* ", Springer, New York, **267** (1992).

33. M. A. Bezerraa, et al., "*Response surface methodology (RSM) as a tool for optimization in analytical chemistry*". Talanta, **76**, 965 (2008).

34. S. J. S. Chelladurai, et al., "*Optimization of process parameters using response surface methodology*": A review. Materials Today: Proceedings, **37,** 1301 (2020).

35. Sh. Karimifard, M. R. A. Moghaddam, "*Application of response surface methodology in physicochemical removal of dyes from wastewater: A critical review*". Science of the Total Environment, **640**, 772 (2018).

36. H. Aghayan, et al., "*Tungsten substituted molybdophosphoric acid loaded on various types of mesoporous silica SBA-15 for application of thorium ion adsorption*". Journal of Nuclear Materials, **496**, 207 (2017).

37. J. Wang, Sh. Zhuang, Y. Liu, "*Metal hexacyanoferrates- based adsorbents for cesium removal*". Coordination Chemistry Reviews, **374**, 430 (2018).

38. M. Chamacka, A. R. Mahjoub, H. Aghayan, "*Catalytic performance of vanadium-substituted molybdophosphoric acid supported on zirconium modified mesoporous silica in oxidative desulfurization*". Chemical Engineering Research and Design, **94**, 565 (2014).

39. H. Aghayan, A. R. Khanchi, A. R. Mahjoub, "*Synthesis and characterization of cesium molybdo vanado phosphate immobilized on platelet SBA-15: An efficient inorganic composite ion-exchanger for gadolinium ion sorption*". Applied Surface Science, **274**, 7 (2013).

40. Z. A. Alothman, "A Review: Fundamental Aspects of Silicate Mesoporous Materials". Materials, **5**, 2874 (2012).

41. S. J. Mousavi, M. Parvini, M. Ghorbani, "*Adsorption of heavy metals (Cu2+ and Zn2+) on novel bifunctional ordered mesoporous silica: Optimization by response surface methodology*", Journal of the Taiwan Institute of Chemical Engineers, **84**,123 (2018).

42. K. D. Kowanga, et al., "*Kinetic, sorption isotherms, pseudo-first-order model and pseudo-second-order model studies of Cu(II) and Pb(II) using defatted Moringa oleifera seed powder*". Journal of Phytopharmacology, **5**, 71 (2016).

43. U. A. Edet, A. O. Ifelebuegu, "Kinetics, Isotherms, and Thermodynamic Modeling of the Adsorption of Phosphates from Model Wastewater Using Recycled Brick Waste". Processes, **8**, 665 (2020).

44. G. Blanchard, M. Maunaye, G. Martin, "*Removal of heavy metals from waters by means of natural zeolites*". Water Research, **18**,1501 (1984).

45. Y. S. Ho, G. Mckey, "*Pseudo-second order model for sorption processes. Process Biochemistry*", **34**, 451 (1998).

46. Y. wang, X. Guo, "*Adsorption isotherm models: Classification, physical meaning, application and solving method*". Chemosphere, **258**, 127279 (2020).

How to cite this article

Sh. Amin, S. A. Alavi, H. Yousefnia, H. Aghayan, *RSM-based Investigation of Cesium Removal from Aqueous Media with Nanocomposites Prepared by Spherical Mesoporous Silica and Potassium Metal Hexacyanoferrate*, Journal of Nuclear Science and Applications, Vol. **3,** No. **2,** P **32-48,** Spring **(2023), Url**: https://jonra.nstri.ir/article_1511.html, **DOI**: 10.24200/jon.2023.0624.